



Surface curvature for measuring sand dune migration based on multi-temporal LiDAR data

Rajshree Rege & Pinliang Dong

To cite this article: Rajshree Rege & Pinliang Dong (2025) Surface curvature for measuring sand dune migration based on multi-temporal LiDAR data, International Journal of Remote Sensing, 46:22, 8856-8877, DOI: [10.1080/01431161.2025.2573243](https://doi.org/10.1080/01431161.2025.2573243)

To link to this article: <https://doi.org/10.1080/01431161.2025.2573243>



Published online: 15 Oct 2025.



Submit your article to this journal [↗](#)



Article views: 39



View related articles [↗](#)



View Crossmark data [↗](#)



Surface curvature for measuring sand dune migration based on multi-temporal LiDAR data

Rajshree Rege and Pinliang Dong

Department of Geography and the Environment, University of North Texas, Denton, TX, USA

ABSTRACT

Accurate measurement of sand dune migration is essential for understanding desert dynamics, climate interactions, and landform evolution. Traditional remote sensing methods using optical satellite imagery often lack the spatial resolution to detect fine-scale dune movements, while existing LiDAR-based techniques such as Pairs of Source and Target Points (PSTP) and Toe Line Tracking (TLT) have limitations related to slipface detection and complexity of processing. This paper introduces a new method that utilizes surface profile curvature to delineate dune toe lines and quantify migration patterns using multi-temporal LiDAR-derived digital elevation models (DEMs) of the White Sands Dune Field (WSDF) in New Mexico, USA. The method identifies toe lines based on extreme positive curvature values, which remain consistent even under wind reversal conditions that obscure slipfaces. Migration distances and rates are estimated by tracking the spatial displacement of toe lines across three LiDAR datasets collected on 24 January 2009, 26 September 2009 and 6 June 2010. Results show average migration rates of approximately 5.1 to 5.5 metres per year, with directionality indicating a bimodal pattern influenced by seasonal wind regimes. Compared to PSTP and TLT methods, the curvature-based approach is more robust in handling dune morphology variations and requires fewer parameters. Spatial variability in migration rates also aligns with vegetation distribution and topographic influences. This curvature-based method improves the automation, reliability and scalability of dune migration analysis, and has potential for broader applications in aeolian geomorphology using high-resolution elevation data.

ARTICLE HISTORY

Received 12 August 2025

Accepted 6 October 2025

KEYWORDS

LiDAR; digital elevation model; sand dune; surface curvature; change detection; White Sands

1. Introduction

Migrating sand dunes have captured the attention of the scientific community for various reasons, including their impact on local human population (Abbasi et al. 2019; Ahmady-Birgani et al. 2017), their interaction with changing climate (Thomas and Wiggs 2008; Tsoar et al. 2009; Wolfe and Hugenholtz 2009; Yizhaq, Ashkenazy, and Tsoar 2009) and their role in shaping the planetary landscape (Hugenholtz et al. 2012; Radebaugh et al. 2010). One of the earliest documented works on sand dunes dates to the late 1800s (Rothrock 1889). Most of these early studies were descriptive and did not mention any

dynamics of sand dune formation and physical processes associated with it. Bagnold's (1941)(Tsoar, H. 1994) milestone work on the physics of sand dunes served as the only guide for researchers for many decades. With the emergence of remote sensing technology, it became possible to study dunes collectively as the dune fields. Breed and Grow (1979) highlights the applications of Landsat images to study the global sand seas. Landsat data has been successfully used to study various dune phenomena such as the impact of seasonal weather, vegetation cover and variations in large scale ($\sim 1 \text{ km} \times 1 \text{ km}$) dune patterns and orientation worldwide. With synoptic coverage of early Landsat data, dune fields could be studied globally but these low- and medium-resolution satellite images could not capture the finer details describing the dune characteristics such as slipfaces, ridges and local dune dynamics.

Hugenholtz et al. (2012) and Zheng et al. (2022) documented recent developments in the remote sensing methods for studying sand dunes. While numerous studies are reported using traditional satellite-based remote sensing techniques (Al-Dabi et al. 1997; Breed, Grolier, and McCauley 1979; Ding, Feng, et al. 2020; Ding, Zhang, et al. 2020; Mohamed and Verstraeten 2012; Pradhan, Moneir, and Jena 2018; Scuderi, Nagle-McNaughton, and Williams 2019), a noticeable shift in the field of sand dune studies became apparent with the usage of Light Detection and Ranging (LiDAR) data (Dong 2015; Dong et al. 2021; Ewing et al. 2008; Saye et al. 2005; Wolfe and Hugenholtz 2009). While satellite data provide synoptic scale coverage of global sand seas, LiDAR data is unique in providing high-resolution (x, y, z) coordinates of ground features with unmatched accuracies.

Taking advantage of the unique capabilities of the LiDAR data, Dong (2015) proposed a Pairs of Source and Target Points (PSTP) method to study dune migration. This method is one of the very few approaches for automatic detection of dune migrations in a dune field. The method uses multitemporal LiDAR Digital Elevation Model (DEM) to identify the dune slipfaces based on the angle of repose ($30\text{--}34^\circ$). However, slipfaces reaching the angle of repose ($30\text{--}34^\circ$) may not develop due to the influence of reverse winds, as shown in Dong et al. (2021). In such scenarios, PSTP may not be able to capture the dune migration accurately. Dune crests are affected more by the change in seasonal wind regime as compared to the dune bases or the toe line position of the dune (Chen et al. 2022). Dong et al. (2021) proposed a new method and named it Toe Line Tracking (TLT) to study dune migration. While dune migration rates using both methods are comparable (for example, TLT produced dune migration rates of 3–8 m/year while PSTP reported migration rates of 4–7 m/year for the White Sands Dune Field), TLT is more robust of the two. The major limiting factor of the PSTP is its dependence on the correct identification of the slipfaces, while TLT successfully overcome this limitation. TLT is based on the identification of interdune polygons. Shift in the position of these polygons is used to estimate the migration distances. Dunes are relatively slow-moving systems. Under the wind, while moving continuously, they try to retain their shape but eventually could evolve into a totally different shape. Depending on sand availability, wind regime and other environmental factors, this transformation could happen at different time scales. In such scenarios, where the data acquisition time interval is substantially higher to witness significant dune transformation for a given dune field, it would be difficult to apply TLT to estimate the dune migrations based on the shift in interdune polygons. Other than this limitation,

TLT is a somewhat complex method that involves some assumptions about the base level height. Although the method is not very sensitive to the choice of these parameters, it adds more steps in the computation because toe lines may be extracted on both stoss slopes and slipfaces of dunes.

To overcome the above limitations, we propose a more direct method to study dune migration based on the identification of the dune toe lines below the slipfaces. This method utilizes the curvature of the dune faces to identify the toe lines. Mathematically, the curvature of any surface can be represented by the second derivative of the surface. While moving along the vertical slope of the dune at the stoss face, which is an upwardly convex surface in many cases, the slope decreases resulting in a negative derivative of the slope. The opposite happens for the slipfaces, which are upwardly concave surfaces. At the toe line of the dune, the surface is upwardly concave. In case of wind reversal, it can be difficult to identify the slipfaces (Dong et al. 2021; Gao, Narteau, and Gadai 2021), but toe lines can still be identified based on the positive curvature of the surface around them. With this relatively consistent nature of the curvature at the toe line, this new method is expected to detect dune migration more accurately.

This paper presents the new method and results obtained from a study area in the White Sands Dune Field (WSDF) in New Mexico, U.S.A., based on multi-temporal LiDAR data. The manuscript is organized into following sections: Introduction, Data and Study Area, Methodology, Results and Discussion, and Conclusions. Results and discussion part includes comparison of results obtained using previous methods. Comparison highlights the strength of the current method along with the limitations.

2. Study area and data

The study area is in the White Sands National Park, New Mexico, U.S.A.. This part of the United States was once a seabed called Permian Sea. Different tectonic activities over the millions of years' time frame resulted in the development of the Sacramento and San Andreas Mountain ranges and Tularosa Basin. Deflation of evaporite beds of Lake Otero and other playa lakes in the basin is the major sediment source of WSDF (Kocurek et al. 2007). During the end of the last ice age snow melts weathered the surrounding mountains and deposited loads of gypsum in the playa lakes located in the basin. Eventually these lakes evaporated resulting in a large gypsum dune field. The park sits in the Tularosa basin sandwiched between the San Andres Mountains on its west and Sacramento mountains on the east. The area of nearly 500 square kilometres in the park is covered by WSDF. The study area of 9 km \times 2.4 km is in the southeast part of the WSDF (Figure 1). Sand dunes in this area are predominantly barchans, transverse and parabolic dunes measuring up to 15 m in height.

WSDF has intrigued the scientific community for a long time and has been very well documented (e.g. McKee 1966; Langford 2003; Ewing, Kocurek, and Lake 2006; Kocurek et al. 2007; R. C. Ewing and Kocurek 2010a, 2010b; Ewing, Hayes, and Lucas 2015). A general orientation of the dune crestlines is found to be NNW (345°) direction with an average spacing of 136 m between the crestlines (Ewing, Kocurek, and Lake 2006). Spring and summers are the windiest months at WDSF with dominant winds from the SW – W, which also explains the general orientation the dune crestlines. During fall and winter winds from N – NW are observed but they are not as strong as compared to the winds

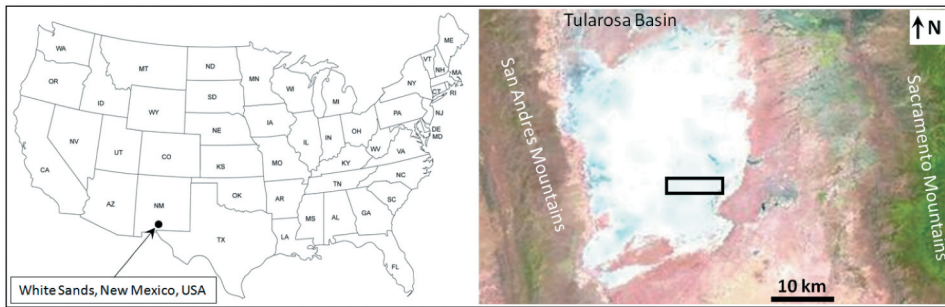


Figure 1. Location of the study area shown as a point on the U.S.A. map. Google earth image of the area surrounding the study is shown on the right panel (Dong 2015).

coming from S-SW direction as observed in spring and summer (Houk and Collier 1994; Kocurek et al. 2007).

The primary data used for this study are LiDAR point cloud data acquired on 24 January 2009, 26 September 2009, and 6 June 2010, and downloaded from the Open Topography Facility (www.OpenTopography.org) at the San Diego Supercomputer Center. The National Center for Airborne Laser Mapping (NCALM: <https://ncalm.cive.uh.edu/>) completed the LiDAR data acquisition and processing. The point density of the three datasets is 4.19 points m^{-2} for 24 January 2009, 5.63 points m^{-2} for 26 September 2009, and 4.62 points m^{-2} for 6 June 2010, and the coordinate system is NAD83 UTM Zone 13N (horizontal), and NAVD88 (vertical). Figure 2 shows the digital elevation models (DEM) created by LiDAR point clouds for the study area for different dates shown. These surfaces are created using Inverse Distance Weighted (IDW) interpolation with a cell size of 1 m \times 1 m. The National Center for Environmental Prediction (NCEP) wind data is used to understand general wind patterns for the study area. National Park Services (NPS) created a vegetation inventory for all the national parks in the United States. NPS inventory for the White Sands National Park (Muldivin et al. 2019) is used to understand the distribution of vegetation and their impact on dune migration in the study area.

3. Methodology

3.1. Mathematical expression of surface curvature

Delineation and analysis of the dune toe line curvature form the mathematical basis for the current study. Curvature of the natural surfaces tells a lot about their evolution and their impact on various surface processes such as erosion, deposition and drainage (Tucker and Bras 1998; Minár, Evans, and Jenčo 2020; Gruber, Baruck, and Geitner 2017). Various methods have been developed to understand the curvature of different surfaces (Peckham 2011; Vinci et al. 2015). Surfaces are two-dimensional objects in a three-dimensional space and can be expressed as a function of x and y coordinates. The surface curvature can be expressed as the second derivative of the surface function. It is, however, simpler to understand the concept of curvature in two dimensions (Figure 3). In Figure 3, let us consider two points A and B located on an irregular cyclic curve $f(x)$. As can be seen,

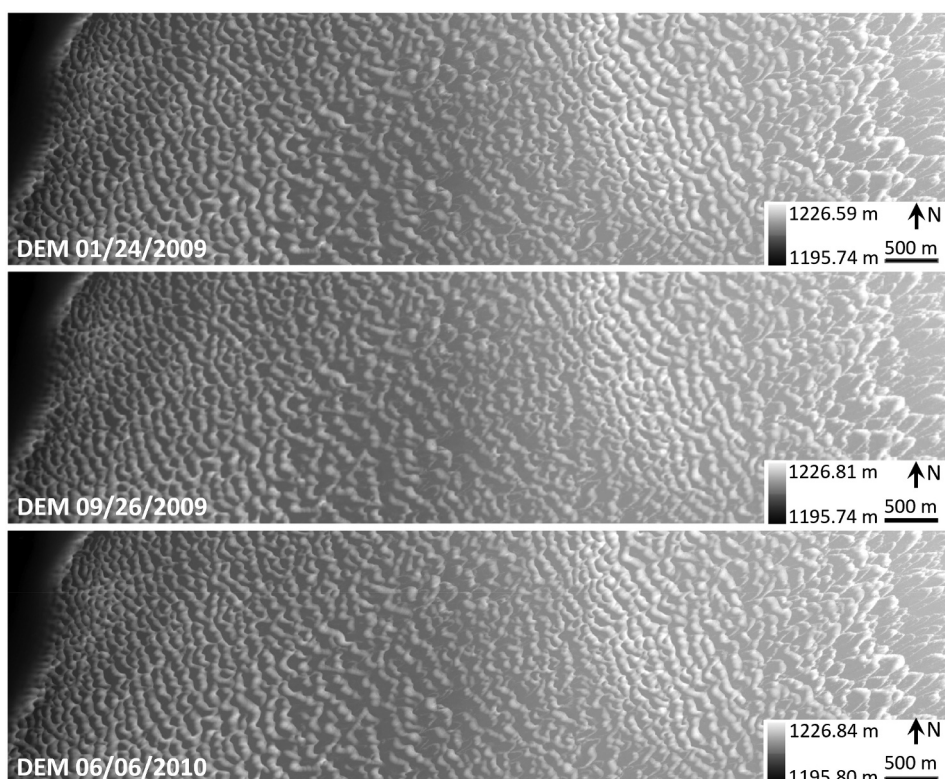


Figure 2. Multi-temporal LiDAR-derived DEMs of the study area (2.4 km \times 9 km) in White Sands, New Mexico, U.S.A. (Dong et al. 2021).

the curvature and orientation of the curve at these two points are different. Any curve can be represented as a part of a circle and the curvature of this curve is expressed as the reciprocal of the radius ($1/\text{radius}$) of the circle. Higher value of the radius of the curve therefore implies less curvature. At point A in Figure 3, the radius of curvature is less as compared to that at point B implying relatively higher curvature at point A.

Although a scalar, curvature can be assigned with a negative or positive sign that helps to understand the orientation of the surface with respect to an observer. In Figure 3, $f(x)$ is a function representing the curve. The tangent at any point on the curve, also known as the slope of the curve at the point, can be represented as the first order derivative, $f'(x)$, of the curve $f(x)$. The second derivative, $f''(x)$ (or the slope of the slope) represents the curvature of $f(x)$. For a straight-line $f'(x)$ is constant resulting in zero curvature. In Figure 3, point A is located at the concave downside of the curve while point B is on the concave upside of the curve. For a concave down curve, the slope of the curve changes in a way that the sign of the second derivative is negative, or, in other words, curvature is negative. On the other hand, for concave upside of the curve the curvature is positive.

The concept of surface curvature in three dimensions is very similar to the two-dimensional description given above but a little more complex. For a surface in three dimensions, curvature at any point can be seen as a combination of curvature along three different planes (Figure 4).

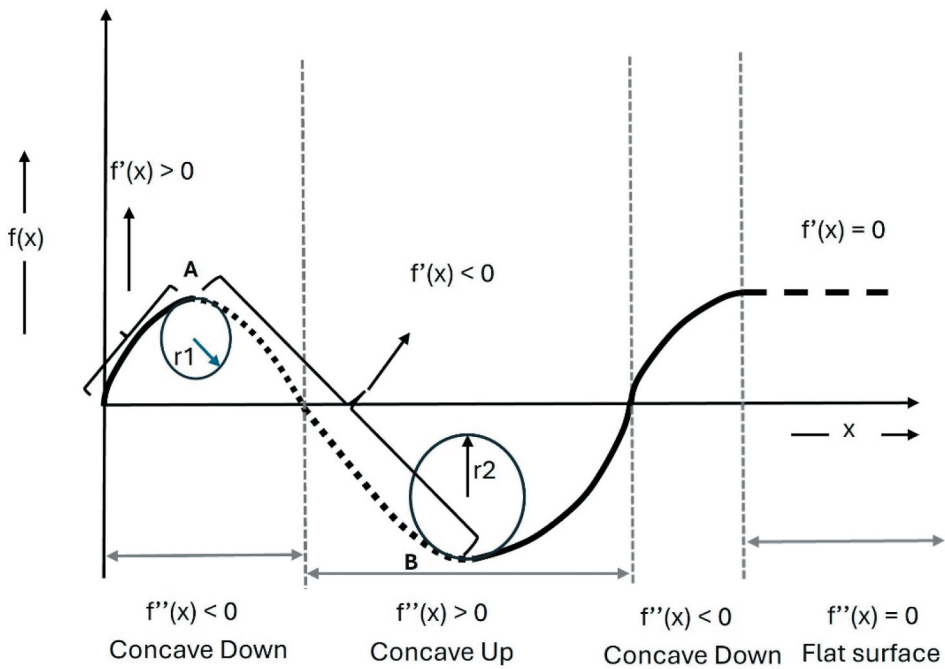


Figure 3. Conceptual diagram explaining curvature in two dimensions.

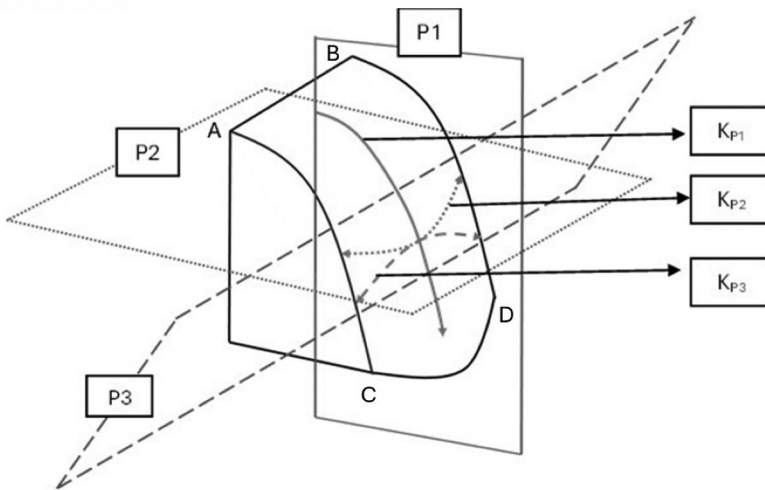


Figure 4. Schematic diagram showing a curved surface in 3-dimensions. Planes P1, P2 and P3 intersect the curved surface ABCD. P1 intersects along the vertically downward slope (shown as the solid line), P2 intersects along the horizontal contour line (shown as the dotted line) and P3 is a plane perpendicular to the plane P2 capturing tangential curvature (shown as dashed line). K_{p1} , K_{p2} and K_{p3} represent the curvatures of the surface along the planes P1, P2 and P3 respectively.

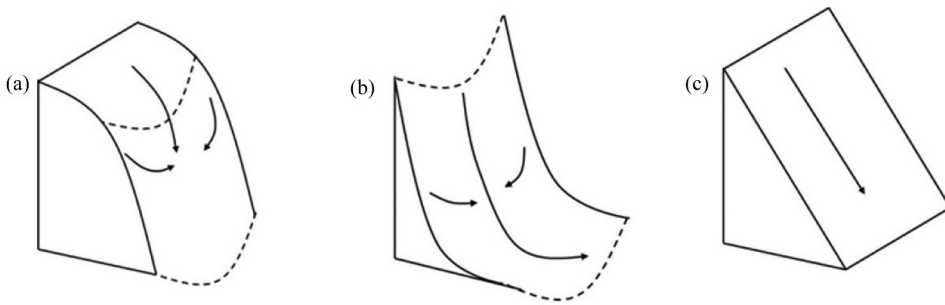


Figure 5. Conceptual diagram explaining curvature. (a) a surface with negative profile curvature and positive plan curvature; (b) a surface with positive profile curvature and positive plan curvature; (c) a flat surface with curvature equals to zero.

In [Figure 4](#), curvature along the plane of the maximum slope or the vertically downward slope of the surface is termed as profile curvature (K_{p1} in plane P1), curvature along a contour in a plane perpendicular to it is termed as plan curvature (K_{p2} in plane P2), and curvature in a plane that is normal to the contour plane is termed as tangential curvature (K_{p3} in plane P3). There could be many different combinations of these three curvatures resulting in many interesting surface orientations. In the schematic diagrams shown in [Figure 5](#), both the curved surfaces (5a and 5b) have positive plan curvature. [Figure 5\(a\)](#) has a negative profile curvature while 5b has a positive profile curvature.

Dune surfaces, like most natural surfaces, are three-dimensional undulating surfaces and can be represented as second- or higher-order polynomials in two variables $f(x, y)$. The tangent at any point on the surface is also known as the slope of the surface at the point and can be calculated by the first derivative of the surface. For a flat surface ([Figure 5\(c\)](#)), the curvature is zero while for a curved surface it will change depending on the orientation of the surface.

Mathematically speaking, if $f(x, y)$ is a function representing a surface, then the expression for the profile curvature (K_{p1}), plan curvature (K_{p2}) and tangential curvature (K_{p3}) can be given as follows ([Peckham 2011](#)):

$$K_{p1} = \frac{f_x^2 f_{xx} + 2f_x f_y f_{xy} + f_y^2 f_{yy}}{(f_x^2 + f_y^2)(f_x^2 + f_y^2 + 1)^{3/2}} \quad (1)$$

$$K_{p2} = \frac{f_y^2 f_{xx} - 2f_x f_y f_{xy} + f_x^2 f_{yy}}{(f_x^2 + f_y^2)^{3/2}} \quad (2)$$

$$K_{p3} = \frac{f_y^2 f_{xx} + 2f_x f_y f_{xy} + f_x^2 f_{yy}}{(f_x^2 + f_y^2)(f_x^2 + f_y^2 + 1)^{1/2}} \quad (3)$$

where,

f_x : First order partial derivative of a function ($f(x, y)$) with respect to x ($\partial f / \partial x$)

f_y : First order partial derivative of function ($f(x, y)$) with respect to y ($\partial f / \partial y$)

f_{xx} : Second order partial derivative of function ($f(x, y)$) with respect to x ($\partial^2 f / \partial x^2$)

f_{yy} : Second order partial derivative of function ($f(x, y)$) with respect to y ($\partial^2 f / \partial y^2$)

f_{xy} : Second order partial derivative of function ($f(x, y)$) with respect to x and y ($\partial^2 f / \partial x \partial y$)

3.2. Surface curvature of sand dunes

Identification of the dune toe lines based on the profile curvature of the dune surfaces forms the basis of the method presented here. A schematic diagram of a barchan dune is given below (Figure 6). Under the influence of wind action, mass transport takes place in the direction of the wind flow. This wind action results in smooth convex up surface (also known as the stoss face) with a gentle slope in the windward side of the dune. The

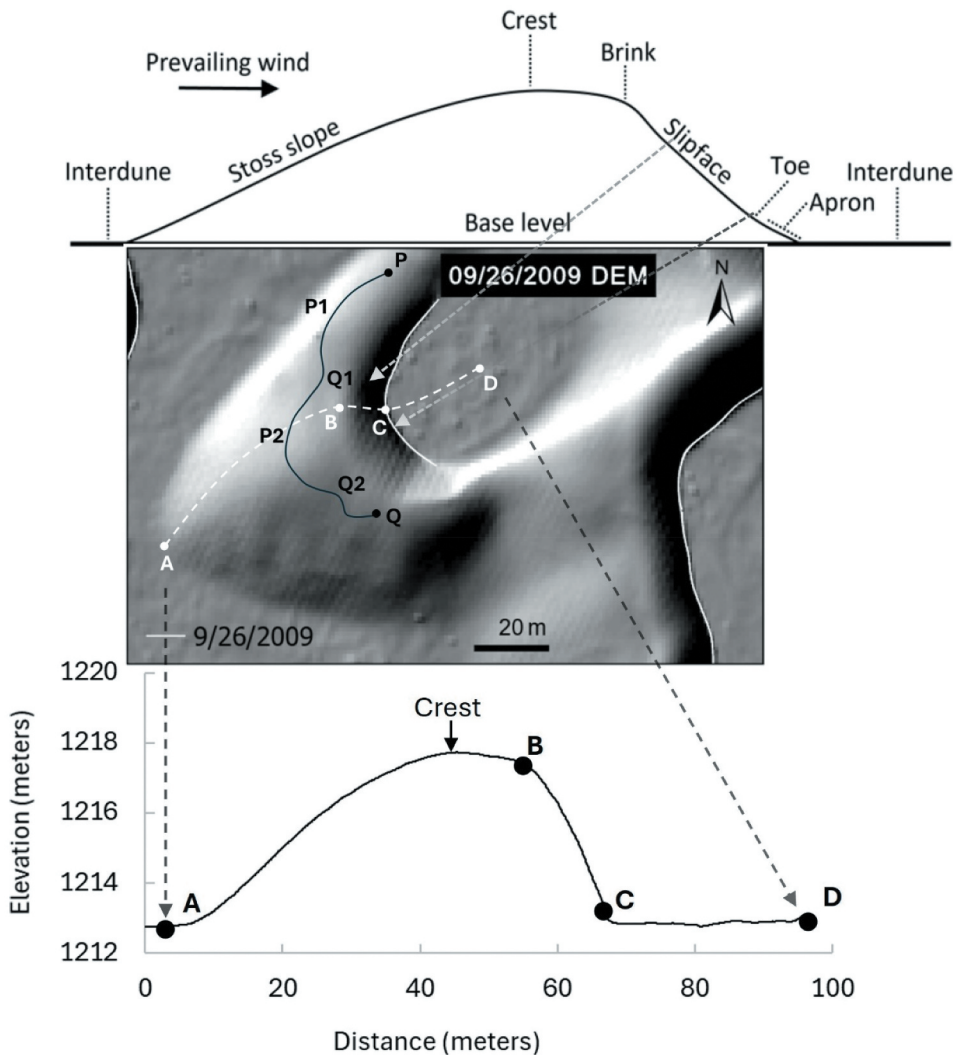


Figure 6. Major parameters of a barchan dune. Top: schematic of a barchan dune (Dong et al. 2021). Middle: 3D view of a dune. Sharp changes in the elevation can be seen along the slipface. Bottom: cross-sectional view of the dune along the line 'ABCD' drawn at random in the direction of the dune's orientation. Point 'C' is nearly 63 metres away from point A, located at the toe line of the dune. The slope and elevation at point C are -64.66% and 1213.05 metres respectively. The elevation at the crest is nearly 1218 metres and the slope is 0.22%. Line PQ is a contour line on the dune stoss face. Along PQ, for segments Q1 and Q2 curvature is positive while for segments P1 and P2 it is negative.

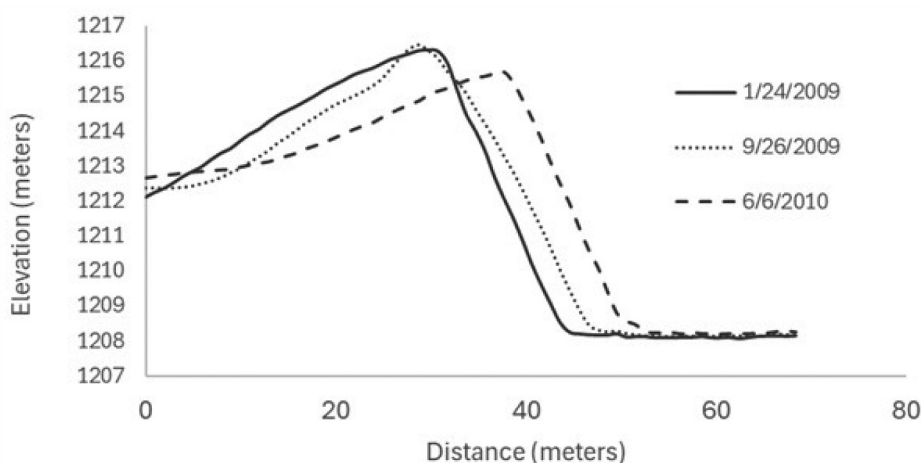


Figure 7. Dune elevation profiles along the prevalent wind direction (NW). Profiles are generated for the same dune with the LiDAR DEMs for three different dates shown in the legend. The profile from 26 September 2009 lacks a slipface near 34° because of reverse wind influence.

leeward surface (also known as the slipface), on the other hand, has a concave up surface with a steep slope. In general, most dunes are oriented perpendicular to the direction of the prevailing wind. Seasonal changes in the wind direction may disrupt this pattern and make it difficult to identify the slipfaces and dune ridges (Figure 7).

Dunes might still be moving in the prevailing wind direction but temporarily may not be tracked based on the position of the slipfaces or the ridges as these features cannot be identified due to wind reversal. Dune toe lines, due to the geometry of the dune, experience the least impact of the reversing winds. Numerical simulations by He et al. (2018) showed that the leeward toe is impacted minimally by the reverse wind action and little sand deposition takes place in this region due to reverse wind flow. This minimal deposition due to reverse wind is not expected to change the direction of curvature of the surface along the toe line. This relatively steady feature of a dune is used to identify dune positions at different points in time.

3.3. Extraction of toe line features

The stoss face of a dune is downward concave with negative profile curvature, as shown in Figure 6 along line AB. As can be seen in Figure 6, plan curvature along contour PQ can be positive (for segments Q1 and Q2) or negative (for segments P1 and P2). Similarly, for the dune slipface the toe line profile curvature is positive, but plan curvature can be either positive or negative depending on the shape of the contour line. Based on this relatively steady nature of the profile curvature at the dune toe line, a method is developed to extract dune toe lines. Temporal shifts in their positions are then used as a proxy for estimating the migration distances and migration rates using multitemporal LiDAR data. A summary of the methodology is presented in Figure 8.

For this study we used the Curvature tool (in ArcGIS Pro) to calculate the profile curvature. With this tool, a zero value for the curvature is indicative of a non-undulating

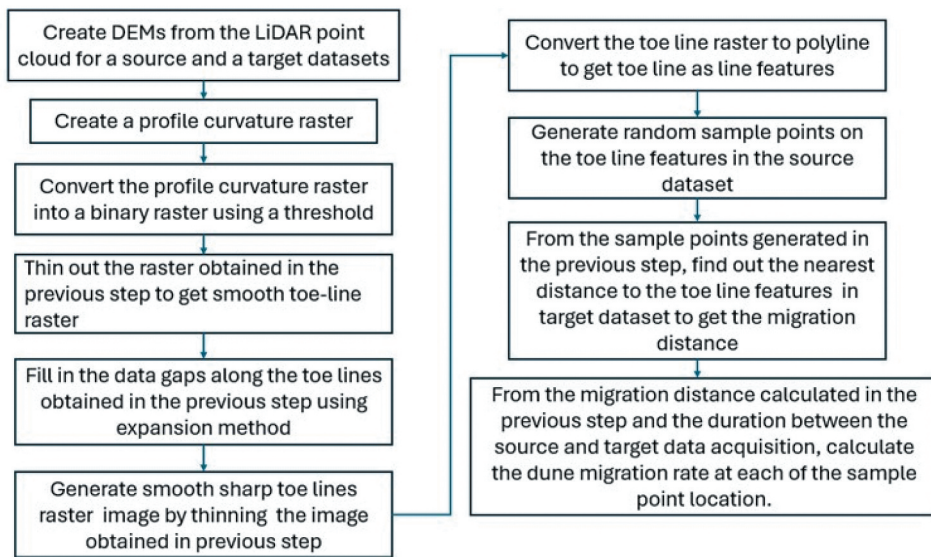


Figure 8. Methodology flowchart for creating toe line features using LiDAR point.

plane whereas a positive (or negative) curvature value is indicative of an upwardly convex (or upwardly concave) surface at the point. Profile curvature for the study area, predominantly fell in the range $(-0.5, 0.5)$. Ridges and toe lines are distinctive features of a dune and can be identified by extreme negative (for the ridges) or extreme positive (for the toe lines) values respectively.

By visual inspection of the DEMs and the histogram of the pixel's values, a curvature value of 20 units is chosen as the threshold for extracting the pixels along the dune toe lines. Thresholds of 10 and 30 are also tested to produce similar toe lines. The only difference between the toe lines extracted using different thresholds is the lengths of the toe lines segments, not the positional accuracy. Therefore, the threshold value is not a major factor influencing the usage of the method. A binary curvature image with curvature ≥ 20 as 1 and curvature < 20 as 0 is created. With the set threshold, some pixels away from the toe lines are also misidentified as value 1 and can be treated as noise in the binary image. To clear this noise from the image, the thinning method is used with default options. Visual inspection of the images at this step reveals some data gaps along the toe lines. To fill in this data gap, the expansion tool in ArcGIS Pro is used, that resulted in somewhat broad toe lines with minimum data gap. To get a smoother toe line raster, thinning tool is applied again. This resulted in a fine toe line with one pixel width. Finally, this toe line raster is converted to polyline features.

3.4. Estimation of migration distances and migration rate

Like any other natural surface, dune features are also irregular in shape and move non-uniformly under the wind action. Parts of the dune that remain in the shadow region of the wind field are less affected by the wind as compared to the parts

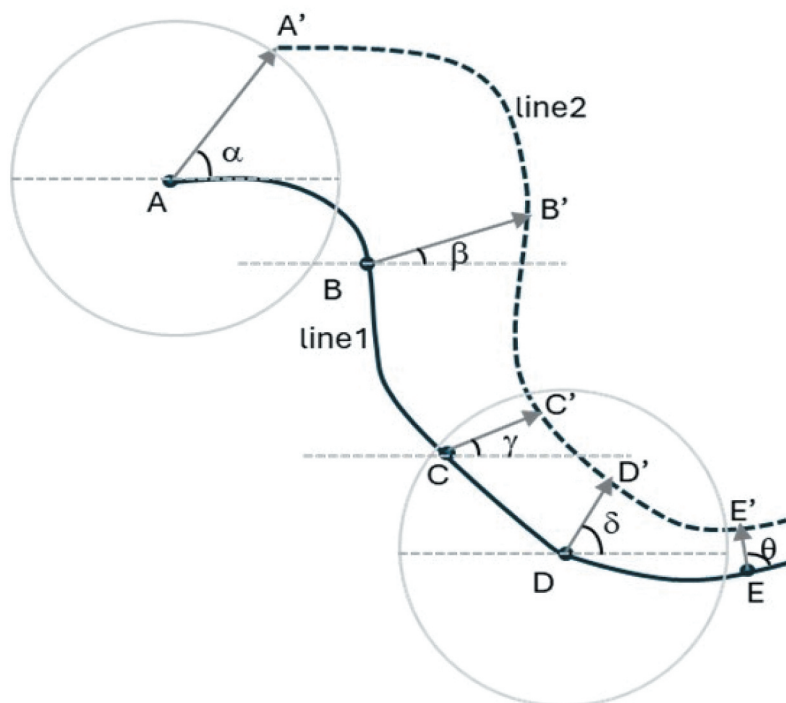


Figure 9. Calculation of dune migration distance and migration direction. line1 represents the toe line feature extracted from the source (or the previous date's data) and line 2 represents the toe line feature extracted from the target (or the later date's data). A, B, C, D and E are random points generated on the source line. The nearest distance from each of these points to the target line within a given search radius is calculated. Angles α , β , γ , δ and θ show the positions of the nearest points on the target line namely A', B', C', D' and E' relative to the source points A, B, C, D and E respectively. These angles give direction of the migration at these points on the dune toe line.

affected directly by the wind. Consequently, displacement in the various parts of the toe lines is also variable depending upon their position with respect to the wind-flow and dune geometry. The toe line can be represented by a set of numerous points. It is logical, therefore, to estimate the shift in the positions of these points to get the estimate of shift in the toe line positions. Random points are generated on the toe lines corresponding to the previous date's data and are termed as the source points. Toe lines corresponding to the later date's data are termed as target lines. The nearest distance between each of the source points and the target line is calculated. This distance can be used as an estimate of the point-wise shift in dune toe line position (Figure 9). The LiDAR data used for the current study is acquired on 24 January 2009, 26 September 2009 and 6 June 2010. That gives us three study periods: 24 January 2009 to 26 September 2009, 26 September 2009 to 6 June 2010, and 24 January 2009 to 6 June 2010.

4. Results and discussion

4.1. Results from a sample area

To demonstrate the workflow of the profile curvature method, [Figure 10](#) shows the results from a small sample area, from the input DEM ([Figure 10\(a\)](#)) to the vectorized toe line ([Figure 10\(h\)](#)).

4.2. Results from the study area

[Figure 11](#) is a sample area showing dune migration. [Figure 11\(d\)](#) shows the toe lines shift from 24 January 2009 to 26 September 2009 to 6 June 2010 on the backdrop of the dune DEM for 6 June 2010. The toe lines can be seen to match the dune landforms very well. Migration distances and directions are shown in [Figure 11\(a\)](#) (from 24 January 2009 to 26 September 2009), [Figure 11\(b\)](#) (26 September 2009 to 6 June 2010) and [Figure 11\(c\)](#) (from 24 January 2009 to 6 June 2010).

As three of these study periods are of different lengths, it is difficult to compare the migration distances for these three periods. Migration distances per year or the migration rates derived using any of the data-pair, however, are expected to be comparable. The number of days in each of the three study periods mentioned above are 245, 253 and 498 respectively. This results in the normalizing factors of 1.4898 (i.e. $365/245$), 1.4427 (i.e. $365/253$) and 0.7323 (i.e. $365/498$), respectively, for the study periods 1, 2 and 3. Migration distances can be converted to migration rates for each of the three pairs of data by multiplying with corresponding normalizing factors. The histogram of migration rates thus generated are shown in [Figure 12](#).

For the first study period which is 245 days long, the histograms are slightly skewed towards relatively lower values with a mean migration rate of 5.47 metres/year. The histograms of migration rates for the second and third period, which are 253 days and 498 days long, are more symmetrical about the mean with mean migration rates rounded to 5.06 metres/year and 5.26 metres/year respectively.

The migration directions for three of the datasets form a bimodal pattern about 75° centred mainly at 45° and 90° respectively ([Figure 13\(d\)](#)). A very small percentage of the total points move outside this directional distribution forming two smaller outer modes ([Figure 13\(d\)](#)). To understand the general wind pattern in the study area, the mean wind patterns for the three study periods are generated using National Centers for Environmental Prediction (NCEP) reanalysis data. Although the NCEP data is available at a coarse resolution (of $2.5^\circ \times 2.5^\circ$), it is useful in depicting the general wind pattern for the study area.

Considering the lag effect of the wind action on dune migration, average wind vector maps are generated starting one month prior to the actual study period. For the first study period, which goes from 24 January 2009 to 26 September 2009, average wind vector map is generated from December 2008 to September 2009. Similarly for the second and third study periods the average wind vector maps are generated for August 2009 to June 2010 and December 2009 to June 2010.

The average wind vector is approximately 75° for three of the study periods. Location of the study area is shown as a red dot on the wind maps. Average wind speed for the first

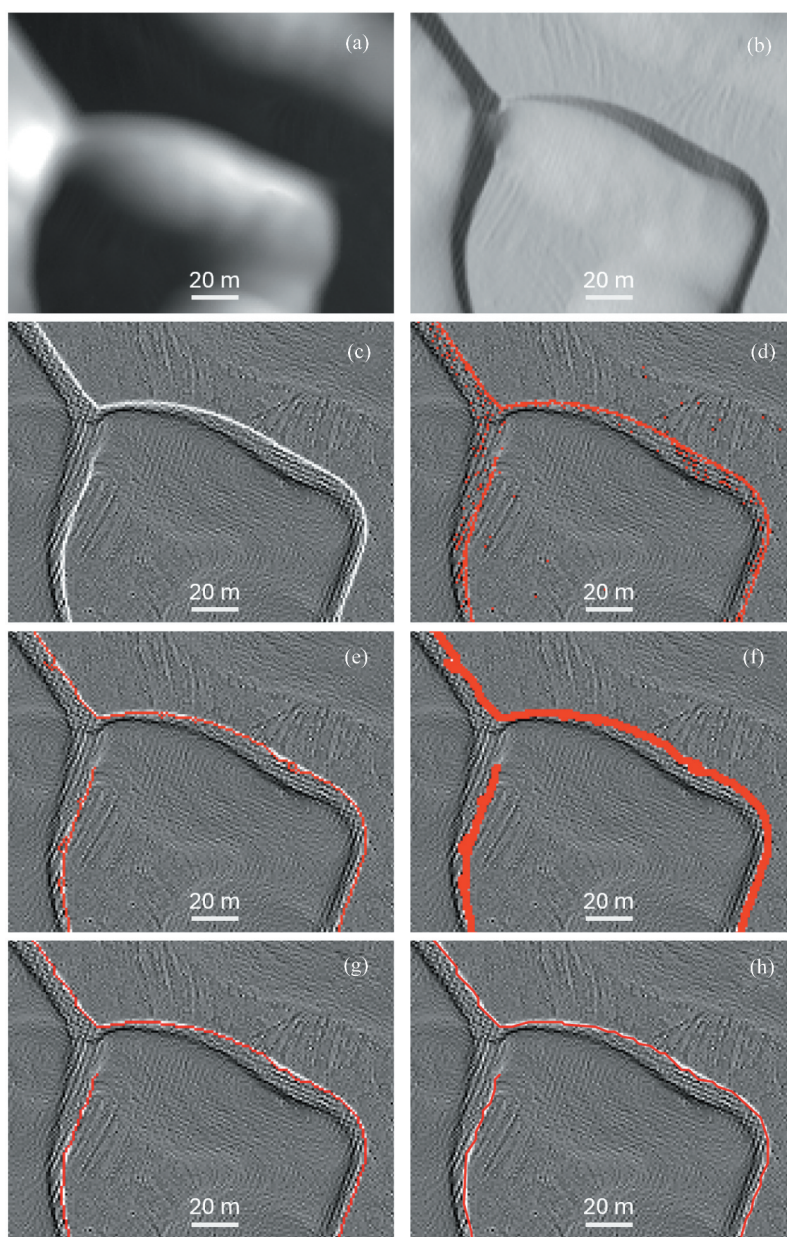


Figure 10. Sample results derived from the DEM of 6 June 2010. (a) DEM of a small area. (b) hillshaded DEM (this is for visualization only). (c) profile curvature raster. (d) binary raster obtained from (c) using 20 as threshold. (e) thinning of (d). (f) expansion of (e). (g) thinning of (f). (h) vectorization (raster to polyline conversion) of (g). Profile curvature raster (10 c) is used as a background for images shown in 10 d through 10 h.

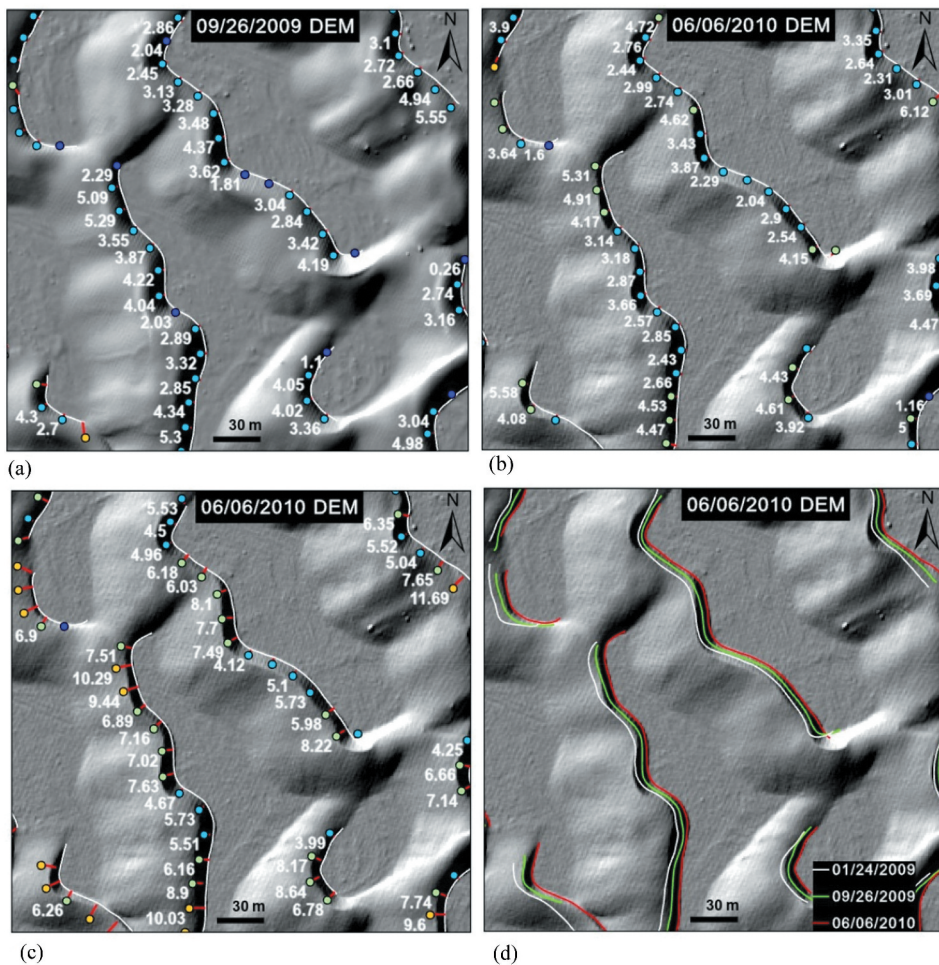


Figure 11. Dune migration distances (in metres) and directions (a) from 24 January 2009 to 26 September 2009; (b) 26 September 2009 to 6 June 2010; (c) 24 January 2009 to 6 June 2010 and (d) sample area showing the shift in toe line position. The backdrops are shaded DEM for the dates mentioned on them.

and third study periods are higher than the second study period. This might explain a little higher estimate of the migration rate (5.47 metres/year and 5.26 metres/year) for these periods as compared to the migration rate estimate (5.06 metres/year) for the second study period. Dune migration represented by random points on the dune seems to have two predominant directions around the prevalent wind direction shown by the dashed arrow in Figure 13(d). This distribution of the migration direction is indicative of a bimodal distribution of wind energy around the prevailing wind direction. This observation is consistent with simulation and field studies primarily done on the ocean wave spectra (Ewans 1998; Toffoli et al. 2010) and needs further exploration specific to the dune fields.

Further migration rate surfaces are created for the study region using the Kriging spatial interpolation method. Migration rates at the sample points are used as the input data with a search radius of 300 m and surfaces are created with a cell size of 120 m × 120

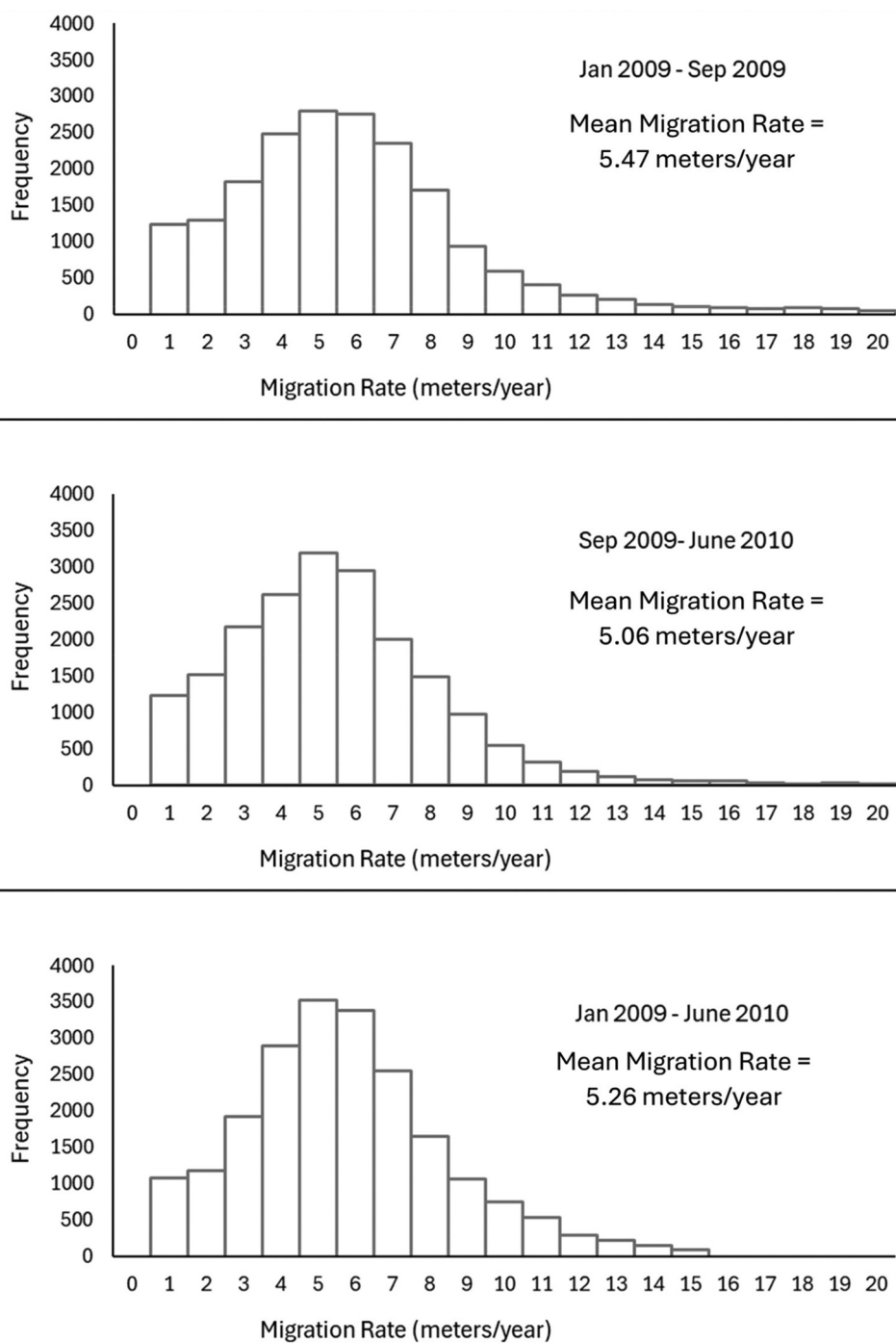


Figure 12. Histograms for dune migration rates for the three study periods.

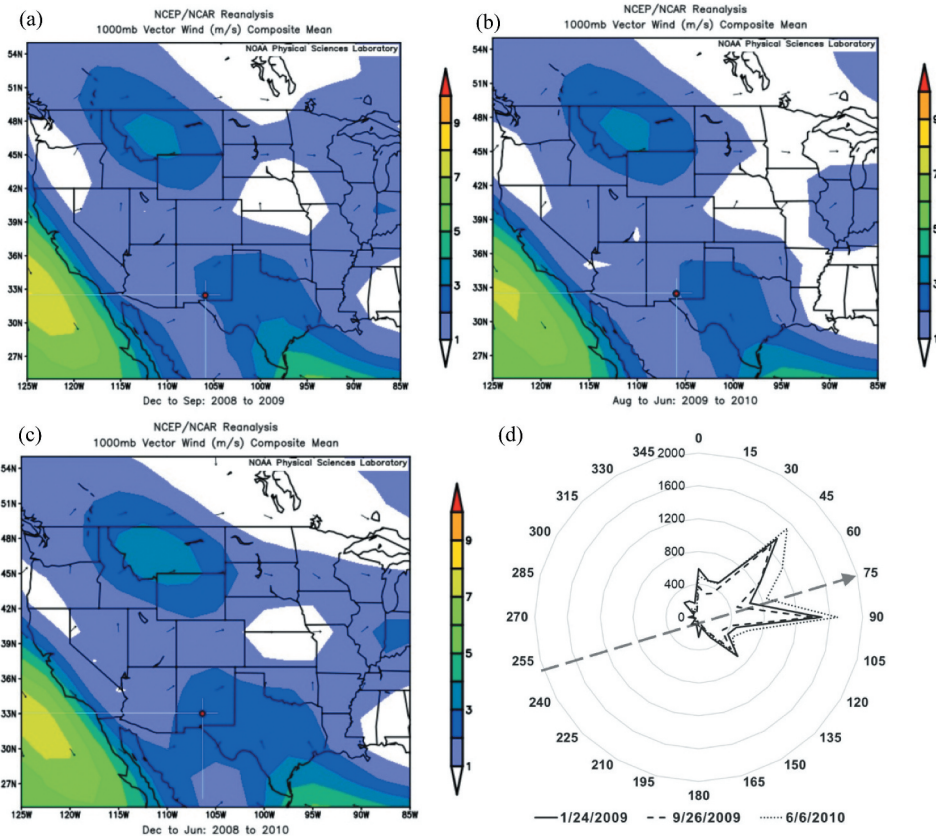


Figure 13. Average surface wind vectors using NCEP wind data for three time periods namely A: Dec 2008 to June 2009, B: August 2009 to June 2010 and C: Dec 2008 to June 2010 are shown. For Figures 13(a-c), wind vector magnitudes range from 1 m/s to 10 m/s. A colour gradient is employed to represent wind vector intensity, with lower magnitudes depicted using cooler colours starting with white and progressing through visible spectrum ending with higher magnitudes indicated by red. Figure 13(d): spider chart showing migration direction of the random points on the dune toe lines, where 0 degrees on the chart represents North. Prevalent wind direction is shown by the dashed arrow.

m. The window size and the search radius for the analysis is kept similar to the TLT method described in Dong et al. (2021). Figure 14 shows the rasters for dune migration rates and vegetation cover in the study area.

One of the National Park Services (NPS) reports, (Muldavine et al., 2019) on vegetation mapping inventory shares vegetation cover data for the White Sands National Park. This data is developed using aerial photographs, Landsat data and land surveys for the national park. A vegetation cover map is generated using this data for the study region. The eastern side of the study area has high vegetation coverage; the western side lacks any vegetation and in the central region moderate vegetation coverage can be seen on the map. Slower migration rates, in the eastern part of the study area can be attributed to the vegetation cover. Migration rates are higher in the western part of the study area. In this region, the base level is upwardly convex, and

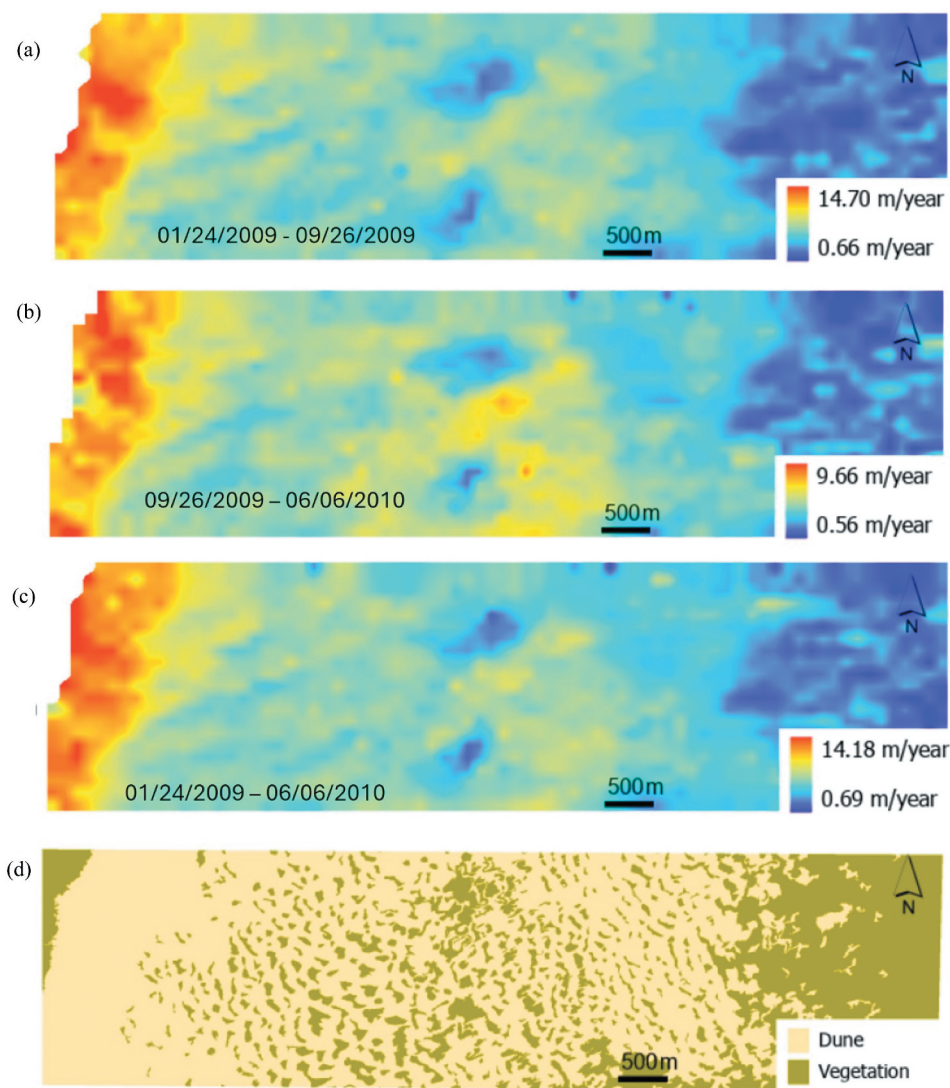


Figure 14. Rasters for dune migration rates and vegetation cover. Spatial maps of migration rates for the study periods (a) 24 January 2009 to 26 September 2009; (b) 26 September 2009 to 6 June 2010 and (c) 24 January to 6 June 2010. (d) vegetation cover map for the study region.

dunes are taller (Dong et al. 2021). Tsoar, White, and Berman (1996) discussed the effect of slope on sand transport and concluded that transport of sand is difficult on an uphill surface which seems contrary to the observations made in the study presented here. It is possible, though, that with more sand accumulation, vegetation growth is impacted negatively that resulted in lack of vegetation in this region and therefore higher migration rates are observed here. The study region base has a slight dip in the central part, which might be a contributing factor in vegetation growth in this region and thus relatively low migration rates. The Eastern part is mostly flat with heavy vegetation cover which explains the lower migration rates in this region.

4.3. Discussion

4.3.1. Comparisons with previous methods

Compared with the previous methods such as PSTP (Dong 2015) and TLT (Dong et al. 2021), the profile curvature method used in this study is more generic in that (1) the profile curvature method can effectively delineate toe lines of sand dunes with or without slipfaces that reach the angle of repose (34°), whereas the PSTP method cannot be applied to sand dunes that do not have slipfaces with an angle of repose close to 34° (Dong et al. 2021); (2) the profile curvature method can effectively detect the toe lines on the leeward side of the dunes, while the TLT method uses a generated surface to cut sand dunes and produce toe lines on both the windward side and leeward side, requiring additional steps to obtain toe lines on the leeward side; and (3) the profile curvature method only needs one parameter (the threshold to extract the toe lines, see Figure 10(c,d), while the TLT methods need multiple parameters. Since the LiDAR datasets were acquired from 2009 to 2010 and the sand dunes are constantly changing, it is not possible to determine which method provides the most accurate results through field validation. Nonetheless, the three methods were based on valid assumptions in morphological development of sand dunes and produced similar results.

Figure 15 is a visual comparison of results from the curvature method and the PSTP method in four selected areas. After generating 3,588 random points on the solid red lines and 3,747 random points on the dashed red lines, distance statistics between the solid red lines and the solid green lines and between the dashed red lines and the dashed green lines are calculated (Table 1). It can be seen that

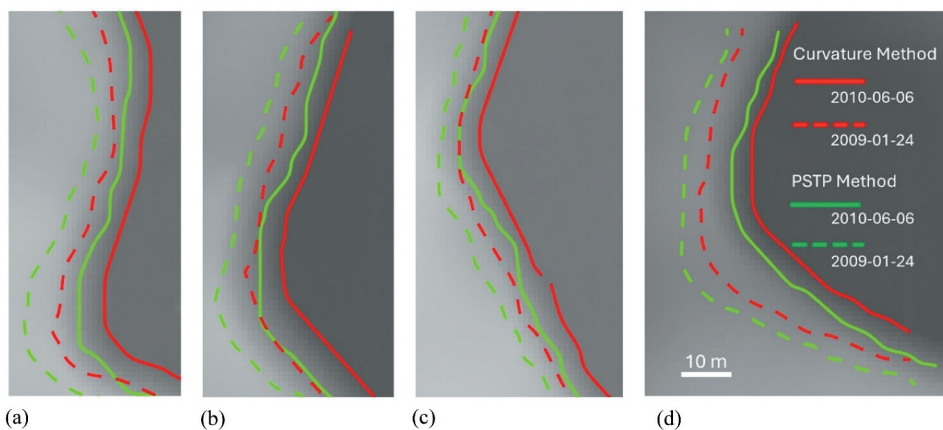


Figure 15. Visual comparison of results from the curvature method and the PSTP method in four selected areas.

Table 1. Statistics of distances between lines derived from the curvature method and the PSTP method.

Dataset	Random Points	Min (m)	Max (m)	Mean (m)	Median (m)	Standard Deviation (m)
2010-06-06	3588	0.02	19.95	5.37	3.97	4.2089
2009-01-24	3747	0.09	19.98	5.22	3.84	4.1454

horizontal distances between corresponding lines derived from the curvature method and PSTP method are less than 4 m at over 50% of random locations. Theoretically, toe lines derived from the TLT method are always between the lines obtained from the slipface-based PSTP method and the lines obtained from the profile curvature method. Therefore, [Figure 15](#) and [Table 1](#) can also be used to analyse results from the TLT method.

4.3.2. Limitations and future improvements

Like the PSTP and TLT methods, the profile curvature method may produce incorrect results when dune migration distances are greater than dune spacings (Dong 2015). Therefore, the time interval between two LiDAR datasets for the same area should be taken into account. To reduce the cost of data collection and increase the temporal resolution of LiDAR datasets, LiDAR sensors on unmanned aerial vehicles (UAV) can be used to collect data along predefined sand dune toe lines, thereby facilitating efficient and accurate mapping of dune migration.

To check if the dune migration direction is consistent with the general wind pattern in the area, we utilized NCEP wind data. While the resolutions of the LiDAR data and NCEP wind data are not comparable, the NCEP wind data gives us an average wind pattern across the study area. With a coarse resolution of $2.5^{\circ} \times 2.5^{\circ}$, this data cannot capture the local variations in wind patterns but serves as a general indicator of prevailing wind. Local wind and local topography have a very dynamic mutual interdependence and would need high-resolution wind data for a detailed study. In this study the focus was to assess the consistency between overall dune migration and the prevailing wind in the region. Since the three LiDAR datasets were acquired in 2009 and 2010 and it is not possible to conduct any field validation due to the changes of the sand dunes, alignment of dune migration rates with the prevailing wind pattern serves as an indirect means to support the results. In the future, higher resolution data can be utilized to better understand the dune migration patterns.

5. Conclusions

This study presents a new, curvature-based method for accurately measuring sand dune migration using multitemporal LiDAR-derived digital elevation models (DEMs). By using surface profile curvature to delineate dune toe lines that remain stable even under varying wind conditions, the proposed method addresses key limitations of earlier techniques such as the Pairs of Source and Target Points (PSTP) and Toe Line Tracking (TLT) methods. Unlike PSTP, which relies on the presence of well-defined slipfaces, and TLT, which depends on the accurate identification of interdune polygons, the profile curvature method offers a simpler, more robust alternative that requires minimal parameter tuning.

The method effectively extracts toe lines based on consistent curvature signatures, which allows reliable detection of dune migration regardless of slipface development, wind reversal, or dune morphology changes such as merging or splitting. Results from the White Sands Dune Field indicate that the method produces migration rates consistent with previous studies (approximately 5.1–5.5 metres/year) and reveals a bimodal migration pattern shaped by seasonal wind regimes.

This approach not only enhances the automation and accuracy of dune migration analysis but also improves scalability for long-term monitoring across diverse dune systems. While further validation using high-temporal-resolution LiDAR data such as drone-based LiDAR data is recommended, especially for rapidly changing dune fields, this curvature-based method represents an important advancement in aeolian geomorphology and landscape analysis based on multi-temporal LiDAR data.

Acknowledgements

Lidar data acquisition and processing completed by the National Center for Airborne Laser Mapping (NCALM – <https://ncalm.cive.uh.edu>). NCALM funding provided by NSF's Division of Earth Sciences, Instrumentation and Facilities Program. EAR-1043051.

Disclosure statement

No potential conflict of interest was reported by the author(s).

Funding

The author(s) reported there is no funding associated with the work featured in this article.

Data availability statement

White Sands National Monument, NM: LiDAR Survey of Dune Fields. Distributed by OpenTopography. <https://doi.org/10.5069/G97D2S2D>. Accessed: 2023–05–29

References

- Ewing, R.C., and G. Kocurek. 2010a. "Aeolian Dune-Field Pattern Boundary Conditions." *Geomorphology*, 114 (3): 175–187.
- Abbasi, H. R., C. Opp, M. Groll, H. Rohipour, and A. Gohardoust. 2019. "Assessment of the Distribution and Activity of Dunes in Iran Based on Mobility Indices and Ground Data." *Aeolian Research* 41:100539. <https://doi.org/10.1016/j.aeolia.2019.07.005>.
- Ahmady-Birgani, H., K. G. McQueen, M. Moeinaddini, and H. Naseri. 2017. "Sand Dune Encroachment and Desertification Processes of the Rigboland Sand Sea, Central Iran." *Scientific Reports* 7 (1): 1523. <https://doi.org/10.1038/s41598-017-01796-z>.
- Al-Dabi, H., M. Koch, M. Al-Sarawi, and F. El-Baz. 1997. "Evolution of Sand Dune Patterns in Space and Time in North-Western Kuwait Using Landsat Images." *Journal of Arid Environments* 36 (1): 15–24. <https://doi.org/10.1006/jare.1996.0230>.
- Bagnold, R. A. 1941. *The Physics of Blown Sand and Desert Dunes*. London: Chapman and Hall.
- Breed, C. S., M. J. Grolier, and J. F. McCauley. 1979. "Morphology and Distribution of Common 'Sand' dunes on Mars: Comparison with the Earth." *Journal of Geophysical Research Solid Earth* 84 (B14): 8183–8204. <https://doi.org/10.1029/JB084iB14p08183>.
- Chen, J., D. Zhang, X. Yang, F. Lehmkuhl, and W. Jiang. 2022. "The Effects of Seasonal Wind Regimes on the Evolution of Reversing Barchanoid Dunes." *Journal of Geophysical Research: Earth Surface* 127 (2): e2021JF006489. <https://doi.org/10.1029/2021JF006489>.
- Ding, C., G. Feng, M. Liao, and L. Zhang. 2020. "Change Detection, Risk Assessment and Mass Balance of Mobile Dune Fields Near Dunhuang Oasis with Optical Imagery and Global Terrain Datasets."

- International Journal of Digital Earth* 13 (12): 1604–1623. <https://doi.org/10.1080/17538947.2020.1767222>.
- Ding, C., L. Zhang, M. Liao, G. Feng, J. Dong, M. Ao, and Y. Yu. 2020. "Quantifying the Spatio-Temporal Patterns of Dune Migration Near Minqin Oasis in Northwestern China with Time Series of Landsat-8 and Sentinel-2 Observations." *Remote Sensing of Environment* 236:111498. <https://doi.org/10.1016/j.rse.2019.111498>.
- Dong, P. 2015. "Automated Measurement of Sand Dune Migration Using Multi-Temporal Lidar Data and GIS." *International Journal of Remote Sensing* 36 (21): 5426–5447. <https://doi.org/10.1080/01431161.2015.1093192>.
- Dong, P., J. Xia, R. Zhong, Z. Zhao, and S. Tan. 2021. "A New Method for Automated Measurement of Sand Dune Migration Based on Multi-Temporal LiDAR-Derived Digital Elevation Models." *Remote Sensing* 13 (16): 3084. <https://doi.org/10.3390/rs13163084>.
- Ewans, K. C. 1998. "Observations of the Directional Spectrum of Fetch-Limited Waves." *Journal of Physical Oceanography* 28 (3): 495–512. [https://doi.org/10.1175/1520-0485\(1998\)028<0495:OOTDSO>2.0.CO;2](https://doi.org/10.1175/1520-0485(1998)028<0495:OOTDSO>2.0.CO;2).
- Ewing, R. C., A. G. Hayes, and A. Lucas. 2015. "Sand Dune Patterns on Titan Controlled by Long-Term Climate Cycles." *Nature Geoscience* 8 (1): 15–19. <https://doi.org/10.1038/ngeo2323>.
- Ewing, R. C., and G. Kocurek. 2010. "Aeolian Dune-Field Pattern Boundary Conditions." *Geomorphology* 114 (3): 175–187. <https://doi.org/10.1016/j.geomorph.2009.06.015>.
- Ewing, R. C., and G. A. Kocurek. 2010b. "Aeolian Dune Interactions and Dune-Field Pattern Formation: White Sands Dune Field, New Mexico." *Sedimentology* 57 (5): 1199–1219. <https://doi.org/10.1111/j.1365-3091.2009.01143.x>.
- Ewing, R. C., G. Kocurek, and L. W. Lake. 2006. "Pattern Analysis of Dune-Field Parameters." *Earth Surface Processes and Landforms: The Journal of the British Geomorphological Research Group* 31 (9): 1176–1191. <https://doi.org/10.1002/esp.1312>.
- Ewing, R. C., G. Kocurek, A. P. B. Peyret, and D. Mohrig. 2008. "Three-Dimensional Characterization and Morphological Dynamics of Gypsum Sand Dunes at White Sands National Monument Using Airborne LiDAR." *Planetary Dunes Workshop* (1403): 31–32 <https://www.lpi.usra.edu/meetings/dunes2008/pdf/7031.pdf>.
- Gao, X., C. Narteau, and C. Gadal. 2021. "Migration of Reversing Dunes Against the Sand Flow Path as a Singular Expression of the Speed-Up Effect." *Journal of Geophysical Research: Earth Surface* 126 (5): e2020JF005913. <https://doi.org/10.1029/2020JF005913>.
- Gruber, F. E., J. Baruck, and C. Geitner. 2017. "Algorithms vs. Surveyors: A Comparison of Automated Landform Delineations and Surveyed Topographic Positions from Soil Mapping in an Alpine Environment." *Geoderma* 308:9–25. <https://doi.org/10.1016/j.geoderma.2017.08.017>.
- He, W., N. Huang, B. Xu, and W. Wang. 2018. "Numerical Simulation of Wind-Sand Movement in the Reversed Flow Region of a Sand Dune with a Bridge Built Downstream." *The European Physical Journal E* 41 (4): 1–9. <https://doi.org/10.1140/epje/i2018-11660-5>.
- Houk, R., and M. Collier. 1994. *White Sands National Monument*. Tucson, AZ, USA: Western National Parks Association.
- Hugenholtz, C. H., N. Levin, T. E. Barchyn, and M. C. Baddock. 2012. "Remote Sensing and Spatial Analysis of Aeolian Sand Dunes: A Review and Outlook." *Earth-Science Reviews* 111 (3–4): 319–334. <https://doi.org/10.1016/j.earscirev.2011.11.006>.
- Kocurek, G., M. Carr, R. Ewing, K. G. Havholm, Y. C. Nagar, and A. K. Singhvi. 2007. "White Sands Dune Field, New Mexico: Age, Dune Dynamics and Recent Accumulations." *Sedimentary Geology* 197 (3–4): 313–331. <https://doi.org/10.1016/j.sedgeo.2006.10.006>.
- Langford, R. P. 2003. "The Holocene History of the White Sands Dune Field and Influences on Eolian Deflation and Playa Lakes." *Quaternary International* 104 (1): 31–39.
1966. "Structures of dunes at White Sands National Monument, New Mexico (and a comparison with structures of dunes from other selected areas) 1." In *Sedimentology* McKee, E. D., 3–69. Vol. 7(1).
- Minár, J., I. S. Evans, and M. Jenčo. 2020. "A Comprehensive System of Definitions of Land Surface (Topographic) Curvatures, with Implications for Their Application in Geoscience Modelling and Prediction." *Earth-Science Reviews* 211:103414. <https://doi.org/10.1016/j.earscirev.2020.103414>.

- Mohamed, I. N., and G. Verstraeten. 2012. "Analyzing Dune Dynamics at the Dune-Field Scale Based on Multi-Temporal Analysis of Landsat-TM Images." *Remote Sensing of Environment* 119:105–117. <https://doi.org/10.1016/j.rse.2011.12.010>.
- Muldavin, E., Y. Chauvin, K. Schulz, T. Neville, P. Neville, J. Smith, and A. Fettes. 2019. Vegetation Classification and Map: White Sands National Monument. *Natural Resource Report. NPS/CHDN/NRR—2019/1906*. Colorado: National Park Service. Fort Collins. <https://irma.nps.gov/DataStore/Reference/Profile/2260027>.
- Peckham, S. D. 2011. "Profile, Plan and Streamline Curvature: A Simple Derivation and Applications." *Proceedings of Geomorphometry* 4:27–30.
- Pradhan, B., A. A. A. Moneir, and R. Jena. 2018. "Sand Dune Risk Assessment in Sabha Region, Libya Using Landsat 8, MODIS, and Google Earth Engine Images." *Geomatics, Natural Hazards and Risk* 9 (1): 1280–1305. <https://doi.org/10.1080/19475705.2018.1518880>.
- Radebaugh, J., R. Lorenz, T. Farr, P. Paillou, C. Savage, and C. Spencer. 2010. "Dunes on Titan and Earth: Initial Remote Sensing Comparisons." *Geomorphology* 121: 122–132.
- Rothrock, J. T. 1889. "The Sand-Dunes of Lewes, Del." *Proceedings of the Academy of Natural Sciences of Philadelphia*, 134–135 <https://www.jstor.org/stable/4061595?seq=1>.
- Saye, S. E., D. Van der Wal, K. Pye, and S. J. Blott. 2005. "Beach–Dune Morphological Relationships and Erosion/Accretion: An Investigation at Five Sites in England and Wales Using LIDAR Data." *Geomorphology* 72 (1–4): 128–155. <https://doi.org/10.1016/j.geomorph.2005.05.007>.
- Scuderi, L., T. Nagle-McNaughton, and J. Williams. 2019. "Trace Evidence from Mars' Past: Fingerprinting Transverse Aeolian Ridges." *Remote Sensing* 11 (9): 1060. <https://doi.org/10.3390/rs11091060>.
- Thomas, D. S., and G. F. Wiggs. 2008. "Aeolian System Responses to Global Change: Challenges of Scale, Process and Temporal Integration." *Earth Surface Processes and Landforms: The Journal of the British Geomorphological Research Group* 33 (9): 1396–1418.
- Toffoli, A., M. Onorato, E. M. Bitner-Gregersen, and J. Monbaliu. 2010. "Development of a Bimodal Structure in Ocean Wave Spectra." *Journal of Geophysical Research Oceans* 115 (C3): C03006. <https://doi.org/10.1029/2009JC005495>.
- Tsoar, H. 1994. "Classics in Physical Geography Revisited." *Progress in Physical Geography: Earth and Environment* 18 (1): 91–96. <https://doi.org/10.1177/030913339401800105>.
- Tsoar, H., N. Levin, N. Porat, L. P. Maia, H. J. Herrmann, S. H. Tatum, and V. Claudino-Sales. 2009. "The Effect of Climate Change on the Mobility and Stability of Coastal Sand Dunes in Ceará State (NE Brazil)." *Quaternary Research* 71 (2): 217–226. <https://doi.org/10.1016/j.yqres.2008.12.001>.
- Tsoar, H., B. White, and E. Berman. 1996. "The Effect of Slopes on Sand Transport — Numerical Modelling." *Landscape and Urban Planning* 34 (3–4): 171–181. [https://doi.org/10.1016/0169-2046\(95\)00235-9](https://doi.org/10.1016/0169-2046(95)00235-9).
- Tucker, G. E., and R. L. Bras. 1998. "Hillslope Processes, Drainage Density, and Landscape Morphology." *Water Resources Research* 34 (10): 2751–2764. <https://doi.org/10.1029/98WR01474>.
- Vinci, A., R. Brigante, F. Todisco, F. Mannocchi, and F. Radicioni. 2015. "Measuring Rill Erosion by Laser Scanning." *Catena* 124:97–108. <https://doi.org/10.1016/j.catena.2014.09.003>.
- Wolfe, S. A., and C. H. Hugenholtz. 2009. "Barchan Dunes Stabilized Under Recent Climate Warming on the Northern Great Plains." *Geology* 37 (11): 1039–1042. <https://doi.org/10.1130/G30334A.1>.
- Yizhaq, H., Y. Ashkenazy, and H. Tsoar. 2009. "Sand Dune Dynamics and Climate Change: A Modeling Approach." *Journal of Geophysical Research: Earth Surface* 114 (F1). <https://doi.org/10.1029/2008JF001138>.
- Zheng, Z., S. Du, H. Taubenböck, and X. Zhang. 2022. "Remote Sensing Techniques in the Investigation of Aeolian Sand Dunes: A Review of Recent Advances." *Remote Sensing of Environment* 271:112913. <https://doi.org/10.1016/j.rse.2022.112913>.